Developmental Biology 349 (2011) 296–309

Contents lists available at ScienceDirect

Developmental Biology

journal homepage: www.elsevier.com/developmentalbiology

# Bim is responsible for the inherent sensitivity of the developing retinal vasculature to hyperoxia

Shoujian Wang [a], SunYoung Park [a], Ping Fei [a], Christine M. Sorenson [b,c,*]

[a] Department of Ophthalmology and Visual Sciences, University of Wisconsin School of Medicine and Public Health, Madison, WI 53792, USA
[b] Department of Pediatrics, University of Wisconsin School of Medicine and Public Health, Madison, WI 53792, USA
[c] UW Eye Research Institute, University of Wisconsin School of Medicine and Public Health, Madison, WI 53792, USA

ARTICLE INFO

*Article history:*
Received for publication 14 June 2010
Revised 7 October 2010
Accepted 26 October 2010
Available online 1 November 2010

*Keywords:*
Angiogenesis
Apoptosis
Retinopathy of prematurity
Choriodal neovascularization
Hyaloid vasculature

ABSTRACT

Apoptosis plays an important role in development and remodeling of vasculature during organogenesis. Coordinated branching and remodeling of the retinal vascular tree is essential for normal retinal function. Bcl-2 family members, such as bim not only influence apoptosis, but also cell adhesive and migratory properties essential during vascular development. Here we examined the impact of bim deficiency on postnatal retinal vascularization, as well as retinal neovascularization during oxygen-induced ischemic retinopathy (OIR) and laser-induced choroidal neovascularization. Loss of bim expression was associated with increased retinal vascular density in mature animals. This was mainly attributed to increased numbers of pericytes and endothelial cells. However, the initial spread of the superficial layer of retinal vasculature and, the appearance and density of the tip cells were similar in bim+/+ and bim−/− mice. In addition, hyaloid vessel regression was attenuated in the absence of bim. Furthermore, in the absence of bim retinal vessel obliteration and neovascularization did not occur during OIR. Instead, normal inner retinal vascularization proceeded independent of changes in oxygen levels. In contrast, choroidal neovascularization occurred equally well in bim+/+ and bim−/− mice. Together our data suggest bim expression may be responsible for the inherent sensitivity of the developing retinal vasculature to changes in oxygen levels, and promotes vessel obliteration in response to hyperoxia.



## Introduction

Apoptosis of vascular cells plays an important role during development, remodeling, and regression of the vasculature and it is tightly regulated by expression of pro- and anti-apoptotic factors (Pollman et al., 1999; Walsh et al., 2000; Wang et al., 2003). Bcl-2 family members affect apoptosis in either a positive or negative manner. Anti-apoptotic mammalian family members share up to four Bcl-2 homology (BH) domains as well as a transmembrane spanning region at the carboxyl end of the protein (Reed et al., 1996). Anti-apoptotic family members include bcl-2, bcl-$X_L$, bcl-w, mcl-1 and A1 (Sorenson, 2004; Strasser et al., 2000; Vaux et al., 1988). Pro-apoptotic members include bcl-2-interacting mediator of cell death (bim), bad, bik, bax and bak. Removal of a single allele of bim is sufficient to prevent the bcl-2−/− phenotype (Bouillet et al., 2001, 2005). Although the role bim plays during embryonic development requires further delineation, its role appears to be a critical one since a significant number of bim−/− and bim+/− mice die prior to embryonic day 9.5 (E9.5) for unknown reasons (Bouillet et al., 1999).

In the mouse, retinal vascular development proceeds following birth. A superficial layer of vessels initiates from the area of the optic disc and spreads radially to the retinal periphery during postnatal day 7. The expanding vessels are immediately covered by the perivascular supporting cells, the smooth muscle cells/pericytes. These vessels sprout deep into the retina and spread perpendicularly to the superficial layer forming the deep and intermediate retinal vessels. Vascularization of the retina is complete by postnatal day 21 but vascular remodeling and pruning continues until postnatal day 48 (Fruttiger, 2007; Wang et al., 2003).

The development of retinal vasculature is tightly coupled to its oxygen needs, and exhibits an inherent sensitivity to fluctuations in oxygen levels. This predisposes the developing retina to retinopathy of prematurity (ROP), which results in ischemia-driven neovascularization of the retina and loss of vision in immature infants exposed to high levels of oxygen to aid lung development and, then brought to room air. Little is known about the cellular and molecular mechanisms involved in inherent sensitivity of the developing retinal vasculature to high oxygen and, more specifically what role bcl-2 family members play during this process. We recently demonstrated significant defects in postnatal retinal vascular development and retinal neovascularization during

* Corresponding author. University of Wisconsin School of Medicine and Public Health, Department of Pediatrics, 600 Highland Avenue, H4/444 CSC, Madison, WI 53792-4108, USA. Fax: +1 608 265 3397.
*E-mail address:* cmsorenson@wisc.edu (C.M. Sorenson).

0012-1606/$ – see front matter © 2010 Elsevier Inc. All rights reserved.
doi:10.1016/j.ydbio.2010.10.034

OIR in bcl-2−/− mice. Retinas from the bcl-2−/− mice exhibited decreased branching and formation of major vessels concomitant with reduced number of endothelial cells (EC), pericytes, and capillaries (Wang et al., 2005). Although bcl-2−/− mice underwent hyperoxia-mediated vessel obliteration they displayed an inability to undergo ischemia-driven neovascularization, despite VEGF expression similar to bcl-2+/+ mice (Wang et al., 2005). Thus, expression of bcl-2 is important during vascular development and angiogenesis, and in its absence VEGF is not sufficient to promote neovascularization.

To gain further insight into the function of bcl-2 in the endothelium we isolated retinal EC from wild-type and bcl-2−/− mice (Kondo et al., 2008). Retinal EC lacking bcl-2 demonstrated reduced cell migration, adhesion and an inability to undergo capillary morphogenesis. In addition, using an *ex vivo* angiogenesis assay we observed reduced sprouting from aortic rings grown in culture from bcl-2−/− mice compared to bcl-2+/+ mice. Mechanistically, bcl-2−/− cells expressed significantly less endothelial nitric oxide synthase (eNOS), an important downstream effector of proangiogenic signaling. This may be attributed to increased oxidative stress in the absence of bcl-2. In fact, incubation of retinal EC or aortic rings from bcl-2−/− mice with the antioxidant N-acetylcysteine restored their capillary morphogenesis and sprouting. Thus, bcl-2-mediated EC functions play important roles not only in survival, but also in proangiogenic phenotype of EC with a significant impact on vascular development and angiogenesis (Kondo et al., 2008). However, little is known regarding the role bim plays in these processes.

Here we determined the impact of bim deficiency on retinal vascular development, retinal neovascularization during OIR, and laser-induced choroidal neovascularization (CNV). In the absence of bim, we observed precocious formation of the retinal vascular plexus, increased density of EC and pericytes, as well as decreased proliferation and apoptosis of vascular cells. Hyaloid vessel regression was also attenuated in the absence of bim. Furthermore, loss of bim expression protected the retinal vasculature from hyperoxia-mediated vessel obliteration and neovascularization during OIR. However, lack of bim expression minimally affected CNV in adult mice. Thus, bim expression modulates retinal blood vessel pruning and remodeling during development, and is responsible for its inherent sensitivity to hyperoxia.

## Materials and methods

### *Tissue preparation*

Bim−/− breeder pairs were obtained from Jackson Laboratory (Bar Harbor, ME) and maintained at the University of Wisconsin animal facilities where our studies were performed according to approved protocols. We maintained this colony by mating heterozygote mutant mice which were genotyped by PCR of genomic DNA extracted from tail biopsies using the following primers 5′-CATTCTCGTAAGTCCGAGTCT-3′, 5′-GTGCTAACTGAAACCAGATTAG-3′ and 5′-CTCAGTCCATTCATCAACAG-3′. For oxygen-induced ischemic retinopathy, 7-day-old (P7) pups and mothers were placed in an airtight incubator and exposed to an atmosphere of 75 ± 0.5% oxygen for 5 days. Incubator temperature was maintained at 23 ± 2 °C, and oxygen was continuously monitored with a PROOX model 110 oxygen controller (Reming Bioinstruments Co., Redfield, NY). Mice were then brought to room air for 5 days, and then pups were sacrificed for retinal wholemount preparations as described below.

### *Trypsin-digested retinal vessel preparation*

Eyes were enucleated from P21 or P42 mice, fixed in 4% paraformaldehyde for at least 24 h. The eyes were bisected equatorially and the entire retina was removed under the dissecting microscope. Retinas were washed overnight in distilled water, and incubated in 3% trypsin (Trypsin 1:250, Difco) prepared in 0.1 M Tris, 0.1 M maleic acid, pH7.8 containing 0.2 M NaF for approximately 1-1.5 h at 37 °C. Following completion of digestion, retinal vessels were flattened by four radial cuts and mounted on glass slides for periodic acid-schiff (PAS) and hematoxylin staining. Nuclear morphology was used to distinguish pericytes from EC. The nuclei of EC are oval or elongated and lie within the vessel wall along the axis of the capillary, while pericyte nuclei are small, spherical, stain densely, and generally have a protuberant position on the capillary wall. The stained and intact retinal wholemounts were coded, and subsequent counting was performed masked.

The number of EC and pericytes was determined by counting respective nuclei under the microscope at a magnification of 400×. A mounting reticle (10 μm × 10 μm) was placed in one of the viewing oculars to facilitate counting. Only retinal capillaries were included in the cell count, which was performed in the mid-zone of the retina. We counted the number of EC and pericytes in four reticles from the four quadrants of each retina. The total number of EC and pericytes for each retina was determined by adding the numbers from the four reticles. The ratio of EC to pericytes was then calculated. To evaluate the density of cells in the capillaries, the mean number of EC or pericytes was recorded in four reticles from the four quadrants of each retina.

### *Visualization of retina vasculature, quantification of avascular area and immunostaining*

Vessel obliteration and the retinal vascular pattern were analyzed using retinal wholemounts stained with anti-collagen IV antibody as described previously (Wang et al., 2003). At various times the eyes of mice were enucleated and briefly fixed in 4% paraformaldehyde (10 min on ice). The eyeballs were fixed in 70% methanol for at least 24 h at −20 °C. Retinas were dissected in PBS and then washed with PBS three times, 10 min each. Following incubation in a blocking buffer (50% fetal calf serum, 20% normal goat serum in PBS) for 2 h, the retinas were incubated with anti-collagen IV (diluted 1:500 in PBS containing 20% fetal calf serum, 20% normal goat serum), GFAP (Dako, Denmark or B4 lectin (Sigma) at 4 °C overnight. Retinas were then washed three times with PBS, 10 min each, incubated with secondary antibody Alexa 594 goat-anti-rabbit (Molecular probes; 1:500 dilution prepared in PBS containing 20% FCS, 20% NGS) for 2 h at RT, washed four times with PBS, 30 min each, and mounted on a slide with PBS/glycerol (2vol/1vol). Retinas were viewed by fluorescence microscopy and images were captured in digital format using a Zeiss microscope (Carl Zeiss, Chester, VA). The central capillary dropout area was quantified, as a percentage of the whole retina area, from the digital images in masked fashion using Axiovision software (Carl Zeiss, Chester, VA).

### *Quantification of neovascular proliferative retinopathy*

Quantification of vitreous neovascularization on P17 was performed as previously described (Wang et al, 2003). Briefly, mouse eyes were enucleated, fixed in formalin for 24 h, and embedded in paraffin. Serial sections (6 μm thick), each separated by at least 40 μm, were taken from around the region of the optic nerve. The hematoxylin and PAS-stained sections were examined in masked fashion for the presence of neovascular tufts projecting into the vitreous from the retina. The neovascular score was defined as the mean number of neovascular nuclei per section found in eight sections (four on each side of the optic nerve) per eye. Vessels of the inner retina were also quantified on these PAS-stained sections.

### *BrdU staining of wholemount retinas*

The detection of cellular proliferation on the retinal blood vessels was assessed by immunohistochemistry for 5-bromo-2-deoxyuridine

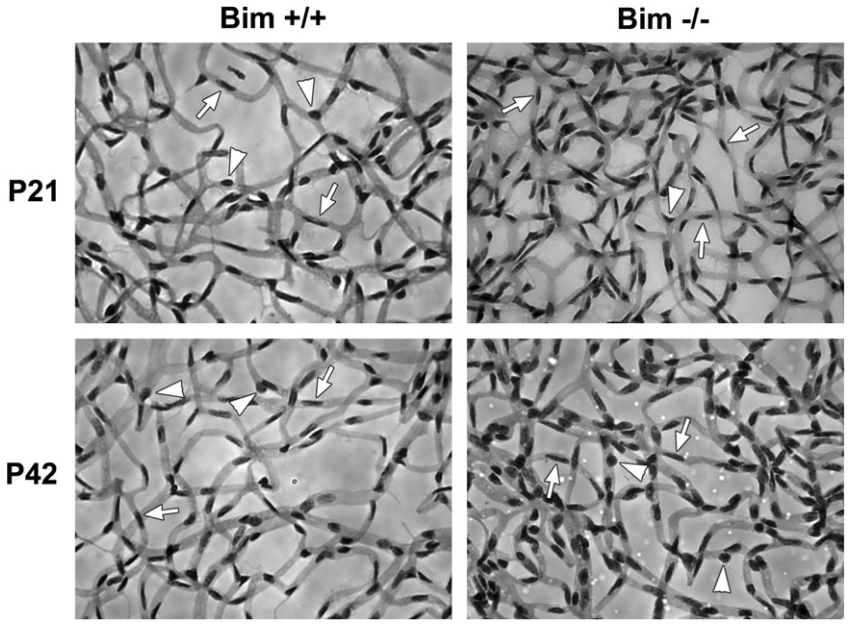


**Fig. 1.** Increased EC and pericyte density in retinas from mature bim−/− mice. Retinas from P21 and P42 bim+/+ and bim−/− mice were prepared by trypsin digest and HE/PAS staining (Wang et al., 2005, 2003). EC and pericytes were then quantified per 100 μm$^2$. Please note that retinas from bim−/− mice demonstrate increased numbers of EC (arrows) and pericytes (arrow heads). Experiments were repeated with eyes from 5 mice with similar results. The quantitative assessment of the data is summarized in Tables 1–3.

(BrdU) incorporation. Mice were injected intraperitoneally with 5-bromo-2-deoxyuridine (BrdU; Sigma, St. Louis, MO) 0.12 g per kilogram of body mass dissolved in water. One and a half hours later the animals were sacrificed, and eyes were removed and fixed immediately in 4% paraformaldehyde for 5 min on ice. Eyes were then transferred to 70% methanol (v/v) and stored at −20 °C for 24 to 72 h. Retinas were dissected in PBS, washed for 30 min in PBS containing 1% Triton X-100 to permeabilize cell membranes, and placed in 2 M HCl at 37 °C for 1 h. Each retina was then washed in 0.1 M sodium borate for 30 min to neutralize the HCl. Retinas were then washed in PBS containing 1% Triton X-100 for 15 min and incubated with a monoclonal antibody to BrdU (Cat No. 1170376, Roche, Indianapolis, IN; diluted 1:250 in PBS containing 1% bovine serum albumin, BSA) at 4 °C overnight or at room temperature for 2 h. Following incubation, retinas were washed for 10 min in PBS containing 1% Triton X-100 and incubated with anti-mouse CY2 antibody (Jackson's Laboratory) diluted 1:500 in PBS containing 1% BSA for 2 h. After a final wash in PBS for 30 min, the retinas were mounted with the ganglion cell layer uppermost in PBS:glycerol (2 vol/1 vol). Retinas were viewed by fluorescence microscopy and images were captured in digital format using a Zeiss microscope (Carl Zeiss, Chester, VA). For quantification, the numbers of BrdU-positive nuclei on the blood vessels were determined per retina.

*Immunohistochemical staining of the frozen sections*

Mouse eyes were enucleated and embedded in optimal cutting temperature (OCT) compound at −80 °C. Sections (9 μm) were cut on a cryostat, placed on glass slides, and allowed to dry for 2 h. For fluorescence microscopy, sections were fixed in cold acetone (4 °C) on ice for 10 min, followed by three washes with PBS, 5 min each. Sections were incubated in blocker (1% BSA, 0.2% skim milk, and 0.3% Triton X-100 in PBS) for 15 min at room temperature. Sections were then incubated with rabbit anti-mouse type IV collagen (Chemicon) (1:500 dilution prepared in blocking solution) overnight at 4 °C in humid environment. After three washes in PBS, 5 min each, sections were incubated with secondary antibody Alexa 594 goat-anti-rabbit (Molecular Probes) (1:500 dilution prepared in blocking solution). Sections were washed three times in PBS, covered with PBS:glycerol (2vol/1vol), and mounted with a coverslip. Retina sections were viewed by fluorescence microscopy, and images were captured in digital format using a Zeiss microscope (Carl Zeiss, Chester, VA).

*TdT-dUTP terminal nick-end labeling (TUNEL) of retinal vessels*

Apoptotic cells were assessed on trypsin digested retinal vessels using TUNEL staining as previously described (Huang et al., 2008). The eyes were removed, fixed in formalin for 48 hours and trypsin digested retina vessels mounted on glass slides. The digests were then washed in PBS, rehydrated, and subsequently washed again. TUNEL staining was performed using a Click-it TUNEL kit (Invitrogen) as recommended by the supplier. The sections were subsequently counterstained with Hoechst 33342 to visualize the nuclei and mounted. Retinal vascular wholemounts were viewed by fluorescence microscopy and the images captured in digital format. A quantitative assessment of the mean number of TUNEL-positive cells was determined per retina.

**Table 1**
EC/PC ratios in Bim+/+ and Bim−/− mice divided according to age (mean ± SD)[†].

| Age, days | Bim+/+ | Bim−/− |
|---|---|---|
| 21 | 2.74 ± 0.45 (8) | 2.63 ± 0.34 (8)[*] |
| 42 | 2.31 ± 0.21 (8) | 2.21 ± 0.25 (8)[*] |

[†] The number of retinas (mice) counted is given in parentheses.
[*] $P>0.05$.

**Table 2**
Number of endothelial cells per reticle square (100 μm$^2$) in Bim+/+ and Bim−/− mice divided according to age (density, mean ± SD)[†].

| Age, days | Bim+/+ | Bim−/− |
|---|---|---|
| 21 | 144.09 ± 12.19 (8) | 219.28 ± 17.26 (8)[*] |
| 42 | 118.72 ± 9.10 (8) | 181.28 ± 18.38 (8)[*] |

[†] The number of retinas (mice) counted is given in parentheses.
[*] $P<0.01$.

**Table 3**
Number of pericytes per reticle square (100 μm$^2$) in Bim+/+ and Bim−/− mice divided according to age (density, mean ± SD)[†].

| Age, days | Bim+/+ | Bim−/− |
|---|---|---|
| 21 | 53.72 ± 7.68 (8) | 84.50 ± 10.10 (8)[*] |
| 42 | 51.81 ± 5.20 (8) | 82.47 ± 7.11 (8)[*] |

[†] The number of retinas (mice) counted is given in parentheses.
[*] $P<0.01$.

*Staining of the hyaloid vasculature*

Following the removal of eyes, the sclera, choroid, and retina were dissected anteriorly from the optic nerve to limbus. The remaining wholemount specimen was stained with FITC-conjugated B4-lectin (1:100 dilution; Sigma, St. Louis, MO) to visualize the hyaloid vasculature. Wholemount specimens were viewed by fluorescence microscopy and images were captured in digital format using a Zeiss microscope (Carl Zeiss, Chester, VA). The dissection resulted, in most

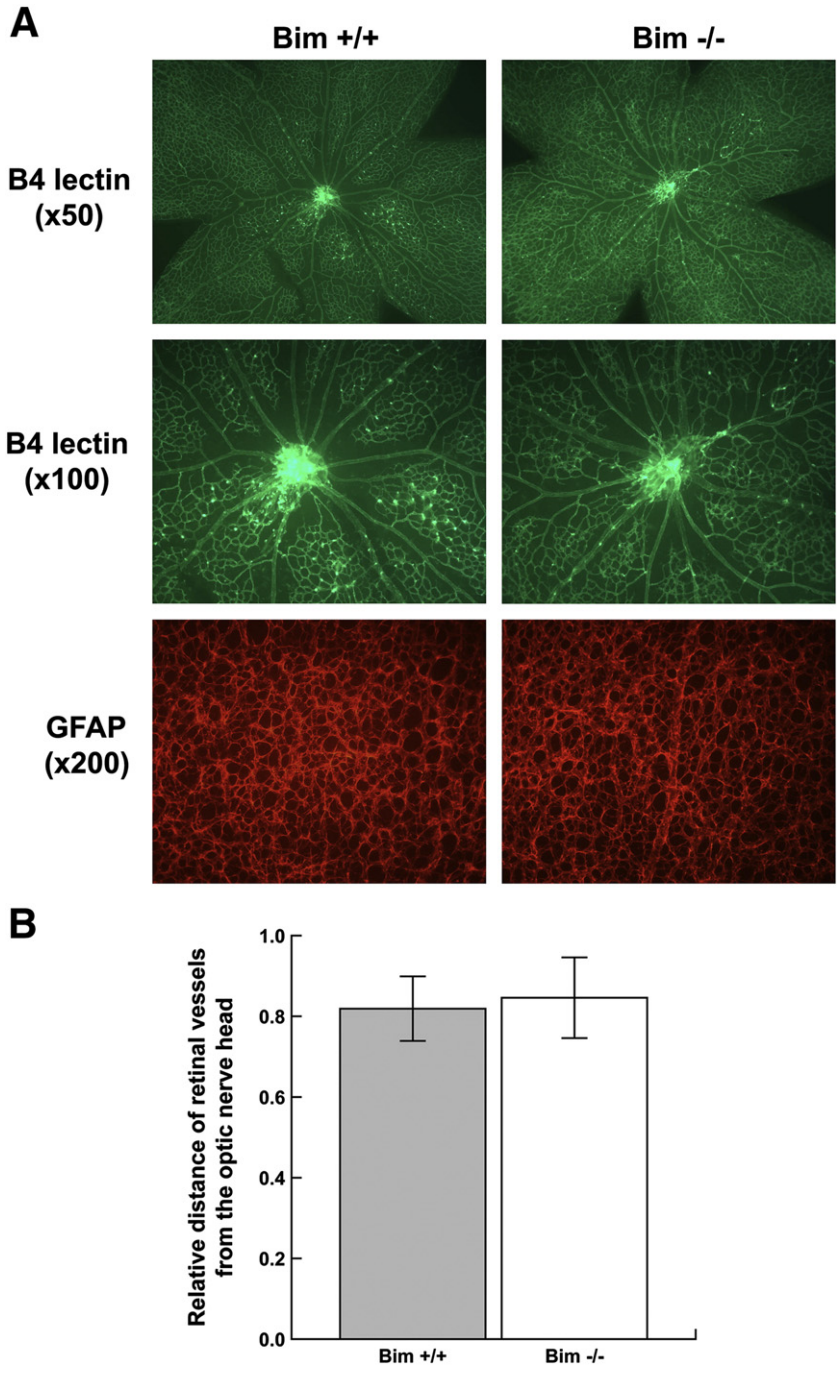


**Fig. 2.** The spreading of superficial retinal blood vessel layer appears similar in P7 bim+/+ and bim−/− mice. In Panel A, assessment of retinal vasculature was performed by wholemount staining with B4 lectin. These experiments were repeated at least three times with eyes from three different mice. Astrocyte density and organization was assessed by GFAP staining. Panel B determines the relative distance the retinal vessels have spread from the optic nerve head. In Panel C, retinas from P5 mice were wholemount stained with B4-lectin and anti-GFAP as noted. Panel D summarizes the mean number of tip cell filopodia per 1 mm vessel length obtained from data presented in Panel C. Please note that the retinal vasculature appears similar in terms of appearance, organization and tip cell density in bim+/+ and bim−/− mice at this time point. Experiments were repeated with eyes from 5 mice with similar results.

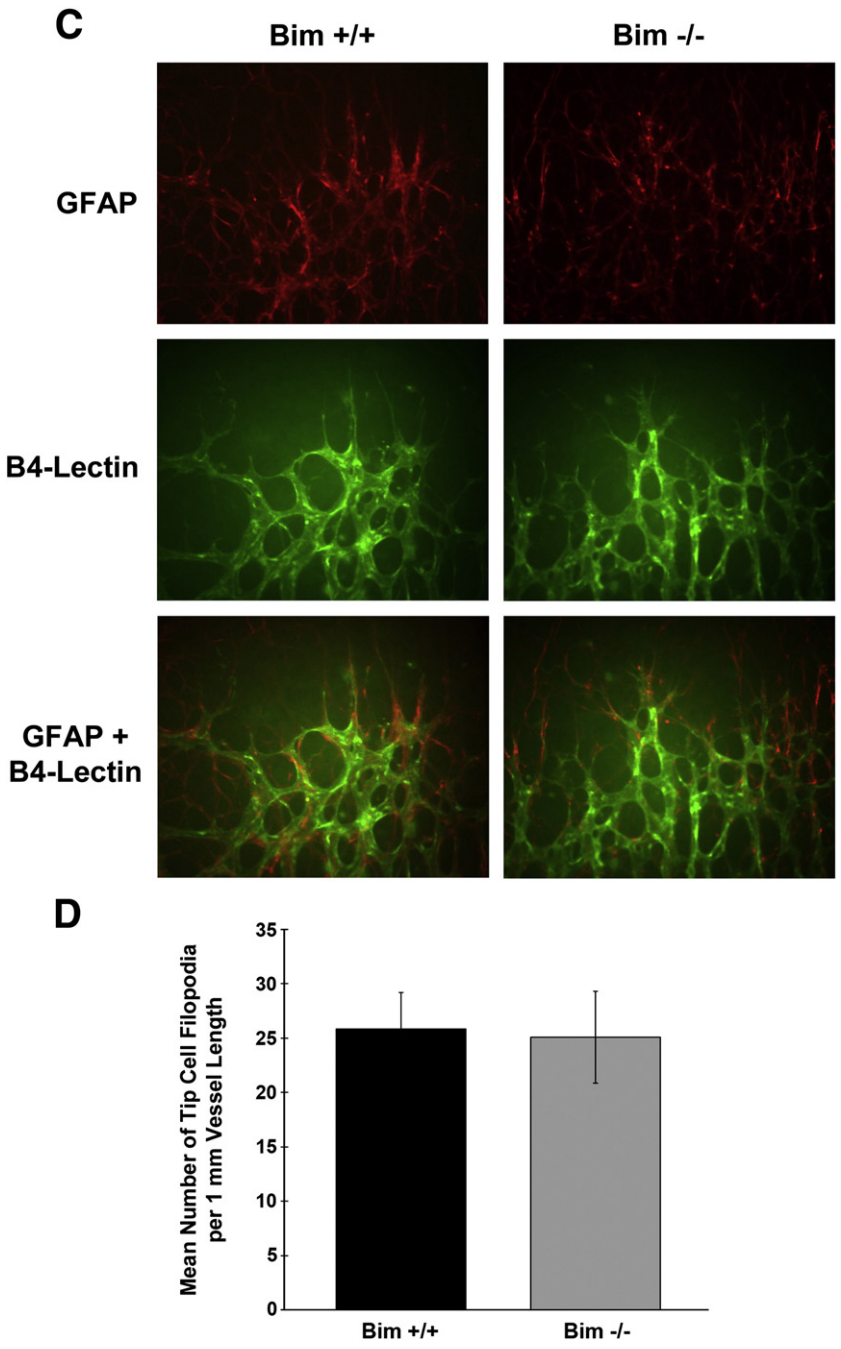


**Fig. 2** (*continued*).

cases, in the loss of hyaloid artery and vasa hyaloidea propria vessels. However, the tunica vasculosa lentis vessels were clearly visible following lectin staining. These experiments were repeated at least three times with eyes from three different mice.

*VEGF analysis*

VEGF protein levels were determined from retina lysate utilizing a mouse VEGF Immunoassay kit (R&D, Minneapolis, MN). Briefly, two retinas were lysed in PBS and the protein concentration of the supernatant determined using a BCA protein assay kit (BioRad). 100 μg of total protein was used in the VEGF Immunoassay, which was performed as recommended by the manufacturer.

*Laser induced choroidal neovascularization (CNV)*

CNV was induced in bim+/+ and bim−/− mice (6 week old, female) by laser photocoagulation-induced rupture of Bruch's membrane on Day 0. Mice were anesthetized with ketamine hydrochloride (100 mg/kg) and the pupils were dilated. Laser photocoagulation (75 μm spot size, 0.1 s duration, 120 mW) was performed in the 9, 12, and 3 o'clock positions of the posterior pole of each eye with the slit lamp delivery system of an OcuLight GL diode laser (Iridex, Mountain View, CA) and a handheld cover slip as a contact lens to view the retina. After 14 days, the eyes were removed and fixed in 4% paraformaldehyde at 4 °C for 2 hours. Following three washes in PBS, the eyes were sectioned at the equator, and the anterior half, the vitreous, and the retina removed. The remaining eye

tissue was incubated in blocking buffer (5% fetal calf serum, 20% normal goat serum in PBS) for 1 hours at room temperature, followed by incubation with anti-ICAM-2 (BD Pharmagen 1:500 in PBS containing 20% fetal calf serum, 20% normal goat serum) overnight at 4 °C. The remaining eye tissue was then washed three times with PBS and incubated with the appropriate secondary antibody. The retinal pigment epithelium–choroid–sclera complex was dissected through five to six relaxing radial incisions and flat mounted on a slide with VectaMount™ AQ (Vector Laboratories, Burlingame, CA). The remaining eye tissue was viewed by fluorescence microscopy and images were captured in digital format using a Zeiss microscope (Zeiss, Chester, VA). Image J software (National Institute of Mental Health, Bethesda, MD; http://rsb.info.nih.gov/ij/) was used to measure the total area (in $\mu m^2$) of CNV associated with each burn.

*Western analysis*

Total protein lysates were prepared from retinas in a modified RIPA buffer (142.5 mM KCl, 5 mM $MgCl_2$ , 10 mM HEPES, pH 7.4, 2 mM orthovandate and 2 mM sodium difluoride, 1% Nonidet P-40, and a complete protease inhibitor cocktail (Roche, Mannheim, Germany)). The proteins were transferred to a nitrocellulose membrane and the membrane was incubated with a rabbit anti-collagen IV. The blot was washed, incubated with appropriate secondary antibody and developed using ECL (Amersham).

*Statistical analysis*

Statistical differences between groups were evaluated with the student's unpaired t-test (two-tailed). Mean ± standard deviation is shown.

## Results

*Bim−/− mice exhibit increased retinal vascular density*

Mouse retinal vasculature develops postnatally and the formation of the primary vascular plexus is complete by P21. However, these vessels continue undergoing pruning and remodeling during the next three weeks maturing by P42. We initially examined the retinal vasculature of P21 and P42 bim+/+ and bim−/− mice. Trypsin digests were prepared to compare retinal vascular densities and EC/pericyte (E/P) ratios in retinas from P21 and P42 bim+/+ and bim−/− mice. The retinal vascular cells were identified based on their nuclear morphology. EC nuclei occur within the vessel wall, are large, oval, and weakly stained and protrude luminally. Pericyte nuclei are darkly stained, small, round, and protrude laterally from the vessel wall. Bim−/− mice demonstrated increased retinal vascular density shown by increased cellularity and capillary loops (Fig. 1). Retinas from P21 and P42 bim−/− mice had increased numbers of EC and pericytes compared to bim+/+ mice (Tables 1 and 2). Since both the numbers of EC and pericytes increased in the absence of bim the E/P ratios for bim+/+ and bim−/− mice were similar (Table 3).

We next determined whether lack of bim affects the early development of retinal vasculature (prior to P21). In the mouse a superficial layer of blood vessels is formed during the first week of postnatal life (P7). These vessels sprout deep into the retina to form the deep and intermediate layer of retina vessels during second and third postnatal week, respectively (Dorrell et al., 2002). We first visualized the developing retinal vasculature by wholemount staining of retinas from P7 mice with either B4 lectin, to specifically stain the vasculature or anti-GFAP to stain astrocytes (Fig. 2A). Astrocytes are a major component of the developing retinal vasculature and provide the scaffolding for the retinal vascular organization, maturation, and remodeling. GFAP staining demonstrated that astrocytes have reached the periphery of the retina in both P7 bim+/+ and bim−/− mice. We also measured the distance that the retinal vessels had spread from the optic nerve head toward the retinal periphery relative to the whole retina radius at P7. Fig. 2B shows the relative distance that the retinal vasculature spread from the optic nerve during the first week of life in bim+/+ and bim−/− mice was similar. We then examined the spreading pattern of astrocytes ahead of the developing vasculature. Fig. 2C demonstrates similar spreading of astrocytes ahead of the developing retinal

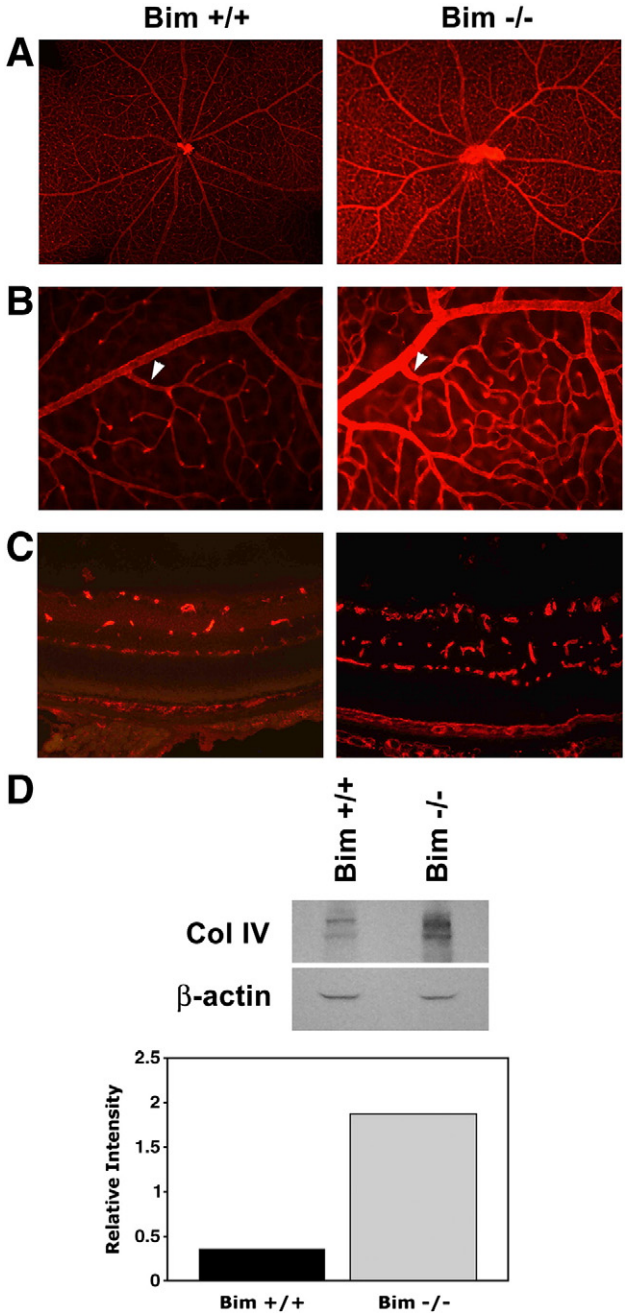


**Fig. 3.** Increased retinal vascular density in the absence of bim. Retinas from P14 bim +/+ and bim−/− mice were wholemount stained with anti-collagen IV at low (50×; Panel A) and high (200×; Panel B) magnification. Photomicrographs are equal timed exposures. Arrow heads point to secondary branches. Please note shortened branch length and tortuous capillaries in retinas from bim−/− mice. In Panel C, retinal histological sections were stained with anti-collagen IV. Protein lysates (40 μg) from bim+/+ and bim−/− mice were analyzed by Western blot analysis for expression of collagen IV (Panel D). β-actin expression was assessed as a loading control. The relative intensity is shown below. Experiments were repeated with eyes from 5 mice with similar results.

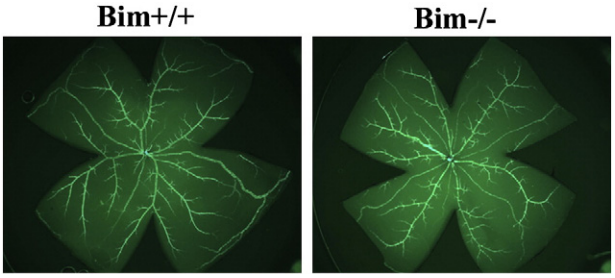


**Fig. 4.** Similar numbers of retinal arteries are present in the presence or absence of bim. Retinas from P21 bim+/+ and bim−/− mice were wholemount stained with anti-α-smooth muscle actin to identify major arteries. Please note that the number of arteries that branch off near the optic nerve were similar in bim+/+ and bim−/− mice. Experiments were repeated with eyes from 5 mice with similar results.

vasculature in P5 bim+/+ and bim−/− mice. We also observed a similar appearance and density of tip cells in the expanding retinal vasculature in P5 bim+/+ and Bim−/− mice (Fig. 2D). Thus, formation of the superficial layer of the retinal vascular layer proceeds similarly in bim+/+ and bim−/− mice.

We next examined the progression of retinal vascularization in P14 mice. We observed increased vascular density, tortuous capillaries and dilated arteries in collagen IV stained retinas from P14 bim−/− mice compared to their wild-type counterpart (Fig. 3A, B). The collagen IV staining of the retinal vasculature was more intense in retinal bim−/− mice compared to bim+/+ mice. In Fig. 3B, a higher magnification of the collagen IV stained wholemount retinas from P14 mice is shown. The arrow heads point to secondary branches which have a shortened branch length in bim−/− mice. Next, retinal histological sections from P14 mice were stained with anti-collagen IV to visualize different layers of retinal vasculature. P14 bim−/− mice demonstrated increased vascularity and formation of the deep retinal vascular plexus compared to bim+/+ mice (Fig. 3C). The increased expression of collagen IV in retinas from P14 bim−/− mice was further confirmed by Western blot analysis (Fig. 3D). Thus, development of the retinal vascular plexus appeared to be enhanced in the absence of bim.

Previous studies from this laboratory demonstrated that in the absence of bcl-2, the number of retinal main arteries and veins were significantly decreased (Wang et al., 2005). We next examined retinas from P21 mice to determine whether bim expression had an impact on the number of retinal arteries and veins. Anti-α-smooth muscle actin mainly stains the major vessels covered by smooth muscle cells and not the capillaries (Fruttiger, 2002). We observed a similar number of major arteries and veins which branch off near the optic nerve in retinas from P21 bim+/+ and bim−/− mice (Fig. 4).

### *Decreased apoptosis and proliferation in the developing retinal vasculature of bim−/− mice*

The increase in density of vascular cells observed in the P14 bim−/− retinal vessels could be the result of decreased apoptosis or increased proliferation during retinal vascularization. The level of apoptosis were determined by TUNEL staining of trypsin digests from retinas of P14 bim +/+ and bim−/− mice. The digests were then co-stained with Hoechst 33342 to identify vascular cell nuclei. We observed a two-fold decrease in the number of apoptotic cells in the retinal vasculature of bim−/−

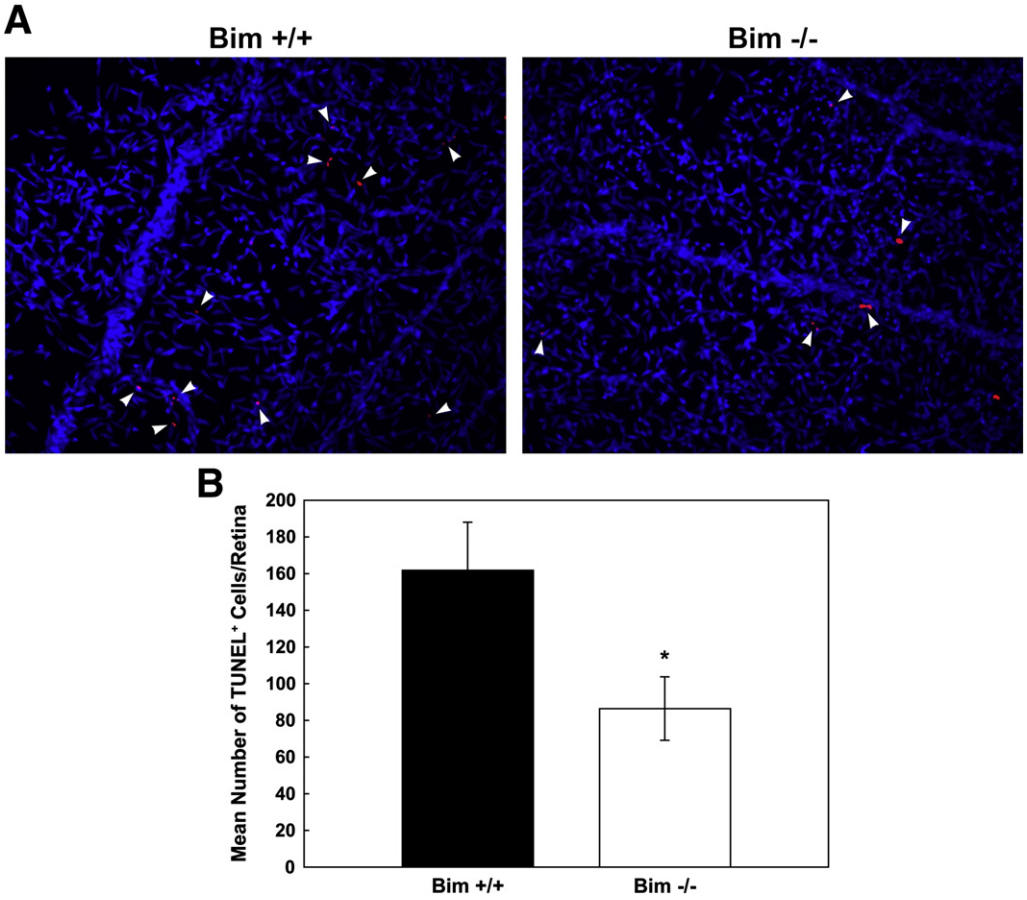


**Fig. 5.** Decreased apoptosis in the absence of bim. The rate of apoptosis of retinal vascular cells was determined by TUNEL staining of trypsin-digested retinal vasculature of P14 bim +/+ and bim−/− mice. The digests were co-stained with Hoechst 33342 to identify nuclei. Apoptotic vascular cells were quantified in Panel B. Please note decreased apoptosis in retinas from P14 bim−/− mice. Experiments were repeated with eyes from 4 mice with similar results.

mice (Fig. 5A). The quantitative assessment of the data is shown in Fig. 5B ($P<0.005$; $n=10$).

Proliferation of vascular cells in the retina diminishes significantly by P21(Huang et al., 2008). P14 is a time point when the maximum amount of proliferation is observed in the wild type mice (Huang et al., 2008; Wang et al., 2005). To determine whether loss of bim expression impacted vascular cell proliferation, P14 bim+/+ and bim −/− mice were injected with BrdU. The retinas were wholemount stained with anti-BrdU and collagen IV (stains blood vessels). Fig. 6 demonstrates that in the absence of bim, proliferation is 15-fold lower than in bim+/+ mice at P14. Fig. 6B is a quantitative assessment of these data ($P<0.05$; $n=15$).

*VEGF expression during retinal vascularization*

VEGF expression by retinal astrocytes has been shown to stimulate retinal vascular development (Stone et al., 1995). Here, we examined VEGF levels in the retina during postnatal retinal vascularization (Fig. 7). VEGF levels in retinas from bim+/+ mice begin a modest decline at P21 and, by P42 the level had declined nearly 4-fold. In the absence of bim, VEGF levels begin a modest decline at P14. At P21, a greater than 2-fold decrease in VEGF expression was observed, such that its expression had declined to near levels observed at P42 in retinas from bim+/+ and bim−/− mice. Although similar VEGF levels were observed early during retina development, VEGF

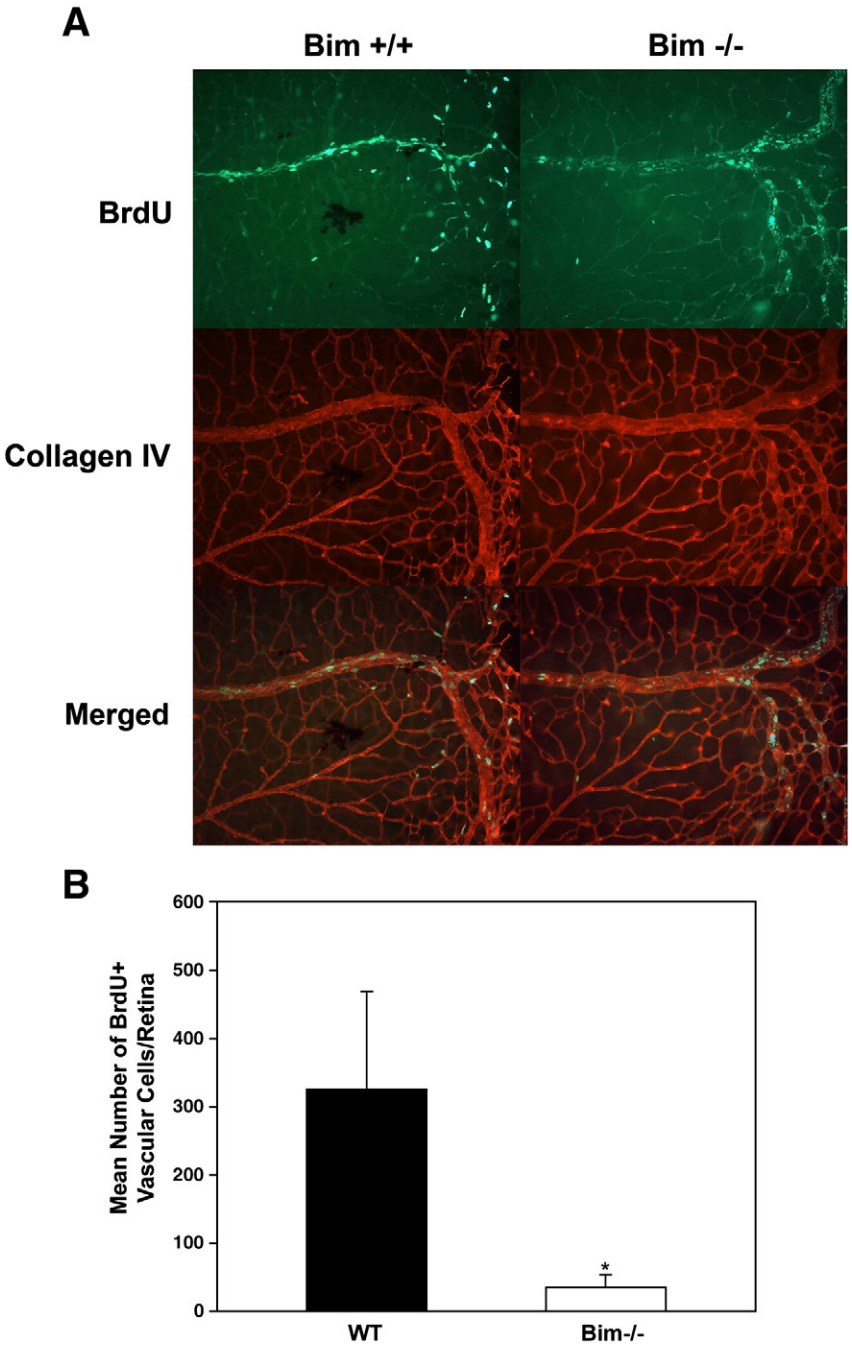


**Fig. 6.** Decreased proliferation in the absence of bim. Proliferating cells in P14 bim+/+ and bim−/− mouse retinas were labeled by BrdU and detected using an antibody to BrdU as previously described (Panel A) (Wang et al., 2005). The data in each bar are the mean number of BrdU+ cells counted in each retina in five eyes of five mice (error bars indicate standard deviation). Please note that the number of proliferating cells is higher in retinas from bim+/+ mice compared to bim−/− mice ($P<0.01$) as quantified in Panel B.

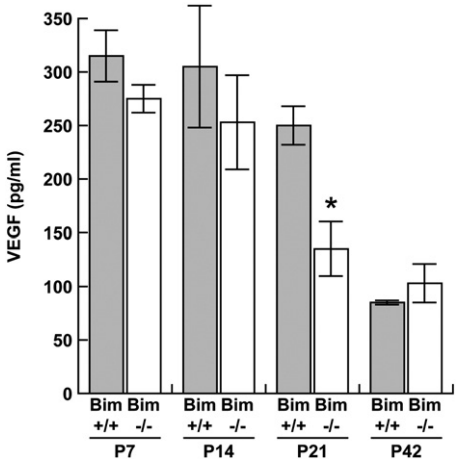


**Fig. 7.** VEGF expression during postnatal retinal vascularization. Retinal lysates (100 μg) were analyzed for VEGF expression. VEGF Immunoassay was used to determine VEGF levels (pg/ml) in retinal lysates from P7 through P42 bim+/+ and bim−/− mice. VEGF levels were determined on retinal lysates from eyes of at least 5 mice with similar results.

expression declined more rapidly in the absence of bim, perhaps due to a reduced need.

*Attenuation of hyaloid vessel regression in the absence of bim*

The pupillary membrane and hyaloid vessels-hyaloid arteries, tunica vasculosa lentis, and vasa hyaloidea propria- provide nourishment to the immature lens, retina, and vitreous (Ito and Yoshioka, 1999). However, they regress during the later stages of ocular development. At P7, bim+/+ and bim−/− mice demonstrated similar development and density of hyaloid vessels (data not shown). Fig. 8 shows the staining of the vasculature in wholemount ocular specimens prepared from bim+/+ and bim−/− mice at six weeks of age. Normally by six weeks of age complete regression of the hyaloid vessels is noted, as we observed in bim+/+ mice (Fig. 8). In contrast, six week old bim−/− demonstrated attenuation of hyaloid vessel regression. These vessels were still evident even in 8-week-old mice (data not shown). Thus, bim expression appears to be essential for retinal hyaloid vessel regression.

*Loss of bim expression prevents hyperoxia-mediated retinal vessel obliteration and neovascularization during OIR*

The inherent sensitivity of the developing retinal vasculature to changes in oxygen level predisposes the retina to ROP. Here, P7 bim +/+ and bim−/− mice were subjected to OIR. At P12, upon return to room air, vessel obliteration in the central area of the retina was assessed. Fig. 9A and B demonstrate that vessel obliteration was absent in bim−/− mice compared to bim+/+ mice. We next determined the degree of neovascularization at P17 by the quantification of vitreous neovascularization as described previously by us (Wang et al., 2005, 2003) and Smith et al (Smith et al., 1994). Hematoxylin and PAS stained sections were examined in a masked fashion for the presence of neovascular tufts projecting into the vitreous from the retina. The neovascular score was defined as the mean number of neovascular nuclei per section found in eight sections (four on each side of the optic nerve) per eye. Consistent with our previous results, bim+/+ mice demonstrated significant neovascularization after 5 days of normoxia, P17 (Fig. 9C, D). However, in the absence of bim we observed little, if any, pathological neovascularization (Fig. 9C, D). Thus, in the absence of bim the developing retinal blood vessels are resistant to hyperoxia-mediated vessel obliteration and vascularization of the inner retina proceeds normally (Fig. 9C; arrow heads in bim−/− mice). Vascularization of the retinal layers following OIR is quantified in Table 4.

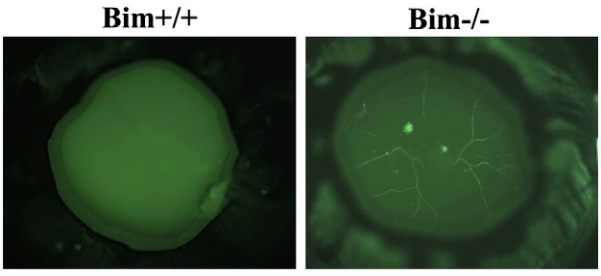


**Fig. 8.** Attenuation of hyaloid vessel regression in the absence of bim. Wholemount staining of hyaloid vessels in P42 bim+/+ and bim−/− mice. Please note complete regression of hyaloid vessels in eyes from bim+/+ mice and attenuation of hyaloid vessel regression in bim−/− mice. Experiments were repeated with eyes from 5 mice with similar results.

VEGF expression is maximally induced during OIR at P15 (Wang et al., 2003). VEGF expression was examined after 3 days of normoxia (OIR at P15), to ensure the lack of neovascularization observed in the absence of bim was not due to decreased VEGF levels. Protein was prepared from retina extracts of P15 bim+/+ and bim−/− mice during OIR. We observed similar levels of VEGF expression in eyes from P15 bim+/+ and bim−/− mice during OIR (Fig. 9E). Thus, the lack of retinal neovascularization during OIR in bim−/− mice was not due to lack of increased VEGF expression in response to hyperoxia followed by normoxia.

*Lack of bim does not affect the development of neural retina*

The potential contribution of bim to the development of the neural retina was examined using retinal sections prepared from P5, P17 and P60 bim+/+ and bim−/− mice (Fig. 10). The thickness, the cellularity, and the organization of retinal layers were similar in bim +/+ and bim−/− mice, in contrast to those previously shown by Doonan et al. (2007). This may be attributed, at least in part, due to differences in tissue fixation and processing. Thus, we did not observed any significant changes in development of the neural retina.

*CNV is not affected in the absence of bim*

CNV appears to share some molecular signals in common with retinal neovascularization. Here, we asked whether lack of bim expression would impact CNV. CNV was induced in P42 bim+/+ and bim−/− female mice by laser photocoagulation-induced rupture of Bruch's membrane on Day 0. The eyes were harvested 2 weeks later and the area of CNV determined by ICAM-2 staining. Fig. 11 demonstrates that the CNV occurred in both bim+/+ and bim−/− mice. Furthermore the area of CNV, as determined by the area of ICAM-2 staining, was not significantly different in the absence of bim ($P>0.05$, $n=20$).

## Discussion

Apoptosis of vascular cells plays an important role in remodeling and regression of the developing vasculature and it is tightly regulated by expression of pro- and anti-apoptotic factors (Pollman et al., 1999; Walsh et al., 2000; Wang et al., 2003). Bcl-2 family members are major regulators of apoptosis, either acting to positively or negatively influence apoptosis. Aberrant regulation of apoptotic pathways impacts retinal vascular development and retinal diseases including ROP, diabetic retinopathy and age-related macular degeneration.

Although coordinated regulation of anti- and pro-apoptotic factors occur during retinal vascular development, only bcl-2's role has been studied in any detail with regards to its modulation by

angiogenic and anti-angiogenic factors. For example, basic fibroblast growth factor (FGF2) and VEGF mediate their proangiogenic effects, partially, through enhanced expression of bcl-2 (Folkman, 2003; Iervolino et al., 2002; Jimenez et al., 2000; Karsan et al., 1997; Sorenson and Sheibani, 2002), while most anti-angiogenic factors, including thrombospondin-1 and endostatin, inhibit angiogenesis through down-regulation of bcl-2 expression (Dias et al., 2002; Giancotti and Ruoslahti, 1999). In addition, over-expression of bcl-2 in EC not only enhances formation of blood vessels but also promotes progressive maturation of vasculature by recruitment of perivascular supporting cells (Giancotti and Ruoslahti, 1999; Kim et al., 2000). However, less is known regarding bim's role. Both insulin-like growth factor-1 and erythropoietin, which are protective during OIR (Chen et al., 2008; Lofqvist et al., 2006, 2009), down-regulate bim expression (Abutin et al., 2009; Linseman et al., 2002). This is also consistent with the protective role of erythropoietin during the first phase of OIR (Chen et al., 2008; Lofqvist et al., 2006), and support a role proposed here for bim in vessel obliteration. Administration of erythropoietin during the second phase of OIR promoted angiogenesis (Chen et al., 2008, 2009). Therefore, bcl-2 family members may function not only as modulators of apoptosis, but also as important regulators of vascular function.

Here, we show that formation of the superficial layer of retinal vasculature appears to proceed similarly in bim+/+ and bim−/− mice. We observed a similar relative distance that the retinal vasculature spread from the optic nerve during the first week of life, as well as the spreading of astrocytes, and appearance and density of tip cells. However, formation of the deep vascular plexus was enhanced consistent with the increased retinal vascular density in the absence of bim. Interestingly, vascular cell proliferation and apoptosis was precociously down-regulated prior to P14 in retinas from bim−/− mice. The decreased apoptosis and proliferation in

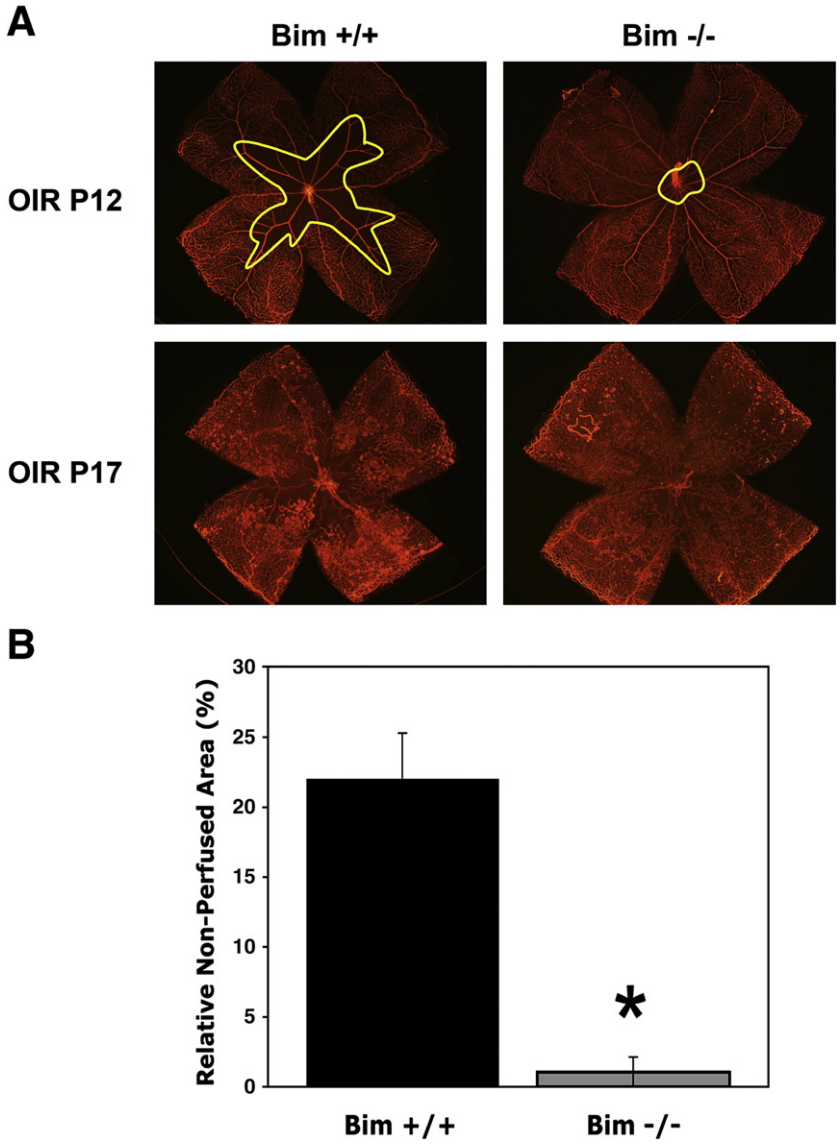


**Fig. 9.** Attenuation of hyperoxia-mediated retinal blood vessel obliteration and neovascularization in the absence of bim. A quantitative assessment of non-perfused area (vessel obliteration; traced area/outlined in yellow) at P12 (5 days of hyperoxia) and neovascularization in P17 mice is shown here (Panel A). Wholemount retinas were stained for collagen IV to visualize the vasculature. The area of vessel obliteration relative to the whole retina was quantified (Panel B). Histological sections from P17 mice (Panel C) were scored for the number of vascular cell nuclei present on the vitreous side of the retina penetrating the inner limiting membrane (Panel D;* $P<0.05$). Note arrows in the vitreous pointing toward vascular tufts. The number of vessels in the superficial, intermediate and deep layers was also determined (Table 4). Arrow heads point to vessels in inner plexiform layer (bim+/+) and outer plexiform layer (bim−/−). Please note that in the absence of bim there is little or no pathologic neovascularization and normal vascularization proceeds even after exposure to high oxygen. Retinal extracts from OIR mice at P15 were subjected to VEGF Immunoassay (Panel E). Please note that VEGF expression was similar following OIR in the presence and absence of bim.

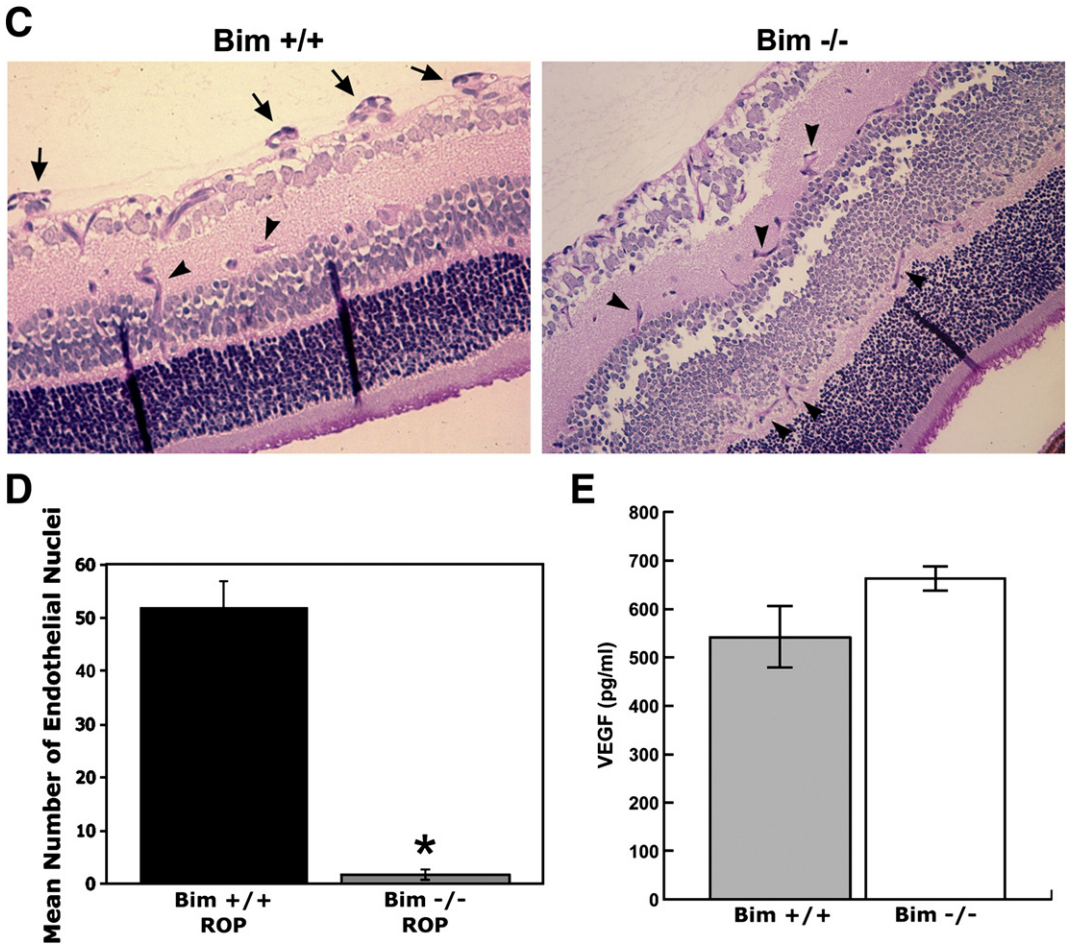


**Fig. 9** (*continued*).

retinas from P14 bim−/− mice was in line with their stage of retinal vascular development rather than postnatal age.

Bcl-2 and bim have been shown to impact not only apoptosis but also cell adhesion, migration and extracellular matrix production (Grutzmacher et al., 2010; Kondo et al., 2008; Sheibani et al., 2007; Ziehr et al., 2004). It is tempting to speculate that, in the absence of bim, the extracellular milieu changes such that vascular sprouting and elongation is accelerated leading to enhanced formation of the deep vascular plexus and perhaps its maturation. This hypothesis is supported by increased levels of collagen IV detected in the retinal vasculature of bim−/− mice.

The development of retinal vasculature is tightly coupled to its oxygen needs and exhibits an inherent sensitivity to changes in oxygen levels. This predisposes the developing retina to ROP, a major cause of blindness in immature infants exposed to high levels of oxygen and then brought to room air. In the mouse OIR model, P7 mice are exposed to 75% oxygen for 5 days, and then returned to room air for 5 days. The exposure of developing retinal vasculature to high oxygen prevents growth of additional vessels and promotes loss of existing vessels due to diminished expression of VEGF, and perhaps the anti-apoptotic protein bcl-2 (Wang et al., 2005). When these mice are returned to room air, the retina becomes ischemic and promotes growth of new vessels, which grow into the vitreous. VEGF expression is maximal 3 days following return to room (P15) and its expression thought to drive abnormal neovascularization in the ischemic retina (Pierce et al., 1996).

**Table 4**
Inner retinal vascularization during OIR in Bim+/+ and Bim−/− mice (mean ± SD)[†].

| Retinal layer | Bim+/+ | Bim−/− |
|---|---|---|
| | P17 OIR | P17 OIR |
| Superficial | 10 ± 1(7) | 21 ± 2(7)* |
| Intermediate | 26 ± 2(7) | 64 ± 4(7)* |
| Deep | 12 ± 1(7) | 29 ± 2(7)* |

[†] The number of retinas (mice) counted is given in parentheses.
* $P<0.01$.

Little is known about the cellular and molecular mechanisms involved in inherent sensitivity of the developing retinal vasculature to high oxygen, and more specifically what role bim plays during this process. Our studies demonstrated that lack of bim expression relieves the retina's inherent sensitivity to high oxygen and ischemia-mediated neovascularization. Hyperoxia-mediated vessel obliteration did not occur in the absence of bim suggesting that bim expression may aid this apoptosis driven process. VEGF expression increases following ischemia and is thought to drive normal retinal vascularization and ischemia-mediated retinal neovascularization (Pierce et al., 1996; Stone et al., 1996, 1995). We had previously observed in bcl-2−/− significant vessel obliteration but decreased neovascularization even though VEGF levels were similar to that of their wild-type counterpart (Wang et al., 2005). Here we show that despite similar VEGF levels in retinas of both bim+/+ and bim−/− mice during OIR, neovascularization did not occur in the absence of bim. Thus, during OIR in bim−/− mice, VEGF expression appears to only drive normal retinal vascularization, while during OIR in bim+/+ mice VEGF expression appears to drive abnormal vascularization (Fig. 9). Bim and bcl-2 expression influences EC migration (Kondo et al., 2008; Grutzmacher et al.,

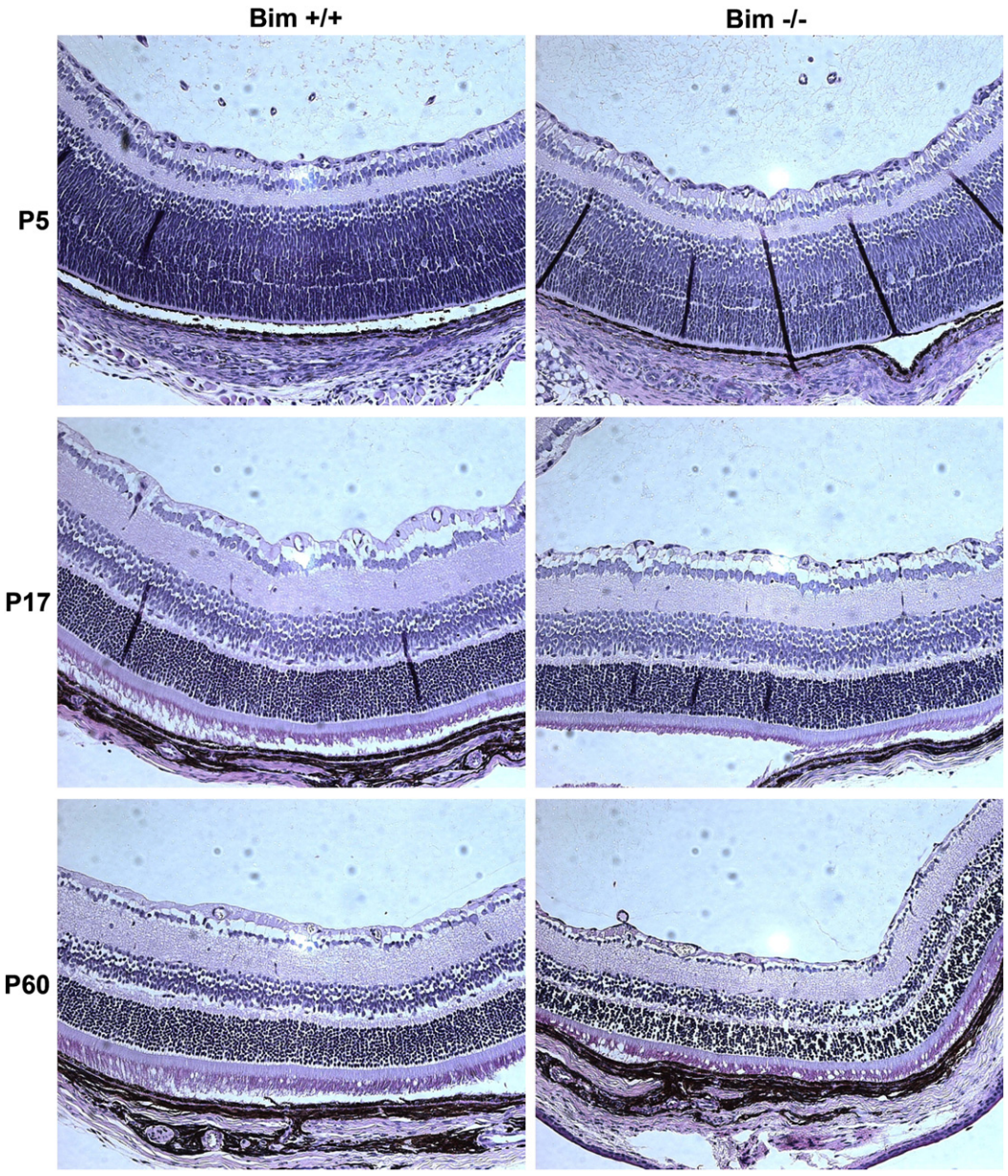


**Fig. 10.** Comparison of retinal section from bim+/+ and bim−/− mice. Eyes were enucleated, fixed and paraffin embedded. Sections (6 μM) were prepared from similar areas and stained with hematoxylin and PAS. Photomicrographs of retinal sections from P5 to P60 bim+/+ and bim−/− mice were taken. These experiments were repeated at least 3 times. Please note that the thickness, cellularity and organization of the retina layers was similar in bim+/+ and bim−/− mice.

2010). Thus, it is tempting to speculate that expression of these proteins may influence or be influenced by directional cues such that either normal retinal vascularization or pathological neovascularization are favored during OIR. These data begin to suggest that VEGF expression, on its own, is not sufficient to drive neovascularization following OIR in the presence or absence of retinal vessel obliteration. Although VEGF has been shown to induce bcl-2 expression little is known regarding its impact on bim expression. Our data suggest that bcl-2 family members may act downstream of VEGF in modulating angiogenesis. To the best of our knowledge, bim is the only gene whose deficiency is shown to protect the developing retinal vasculature from sensitivity to hyperoxia.

Exposure to high oxygen prevents formation of the retinal deep vascular plexus during OIR. However in the absence of bim, vascularization of the inner retina proceeded rather normally. This is perhaps due to the lack of hyperoxia-mediated vessel obliteration or a unique ability of bim−/− EC to circumvent hyperoxia-mediated inhibition of normal angiogenesis. In addition, these data may begin to hint at the mechanism by which retinal vascular pruning is modulated by bim. Normally vascular pruning occurs when an overabundance of oxygen triggers a drop in VEGF expression. Perhaps, hyperoxia-mediated vessel obliteration could be considered retinal vascular pruning gone arye. Our data suggest that bim expression facilitates vascular pruning and remodeling. In the absence of bim, changes in oxygen and/or VEGF levels are not sufficient to induce pruning as evidenced by the increased vascular density, EC numbers and attenuation of hyaloid vessel regression in bim−/− mice.

The retina can undergo two types of neovascularization: retinal neovascularization and CNV, as occurs in retinopathy of prematurity and age-related macular degeneration, respectively. Unfortunately, the molecular and cellular mechanisms involved in CNV have not been studied to the same degree as retinal neovascularization. Although these processes are thought to share molecular signals, the role hypoxia plays during CNV remains questionable (Campochiaro, 2000). Retinal neovascularization was not observed during OIR in bim−/− mice while laser-induced CNV occurred in the absence of

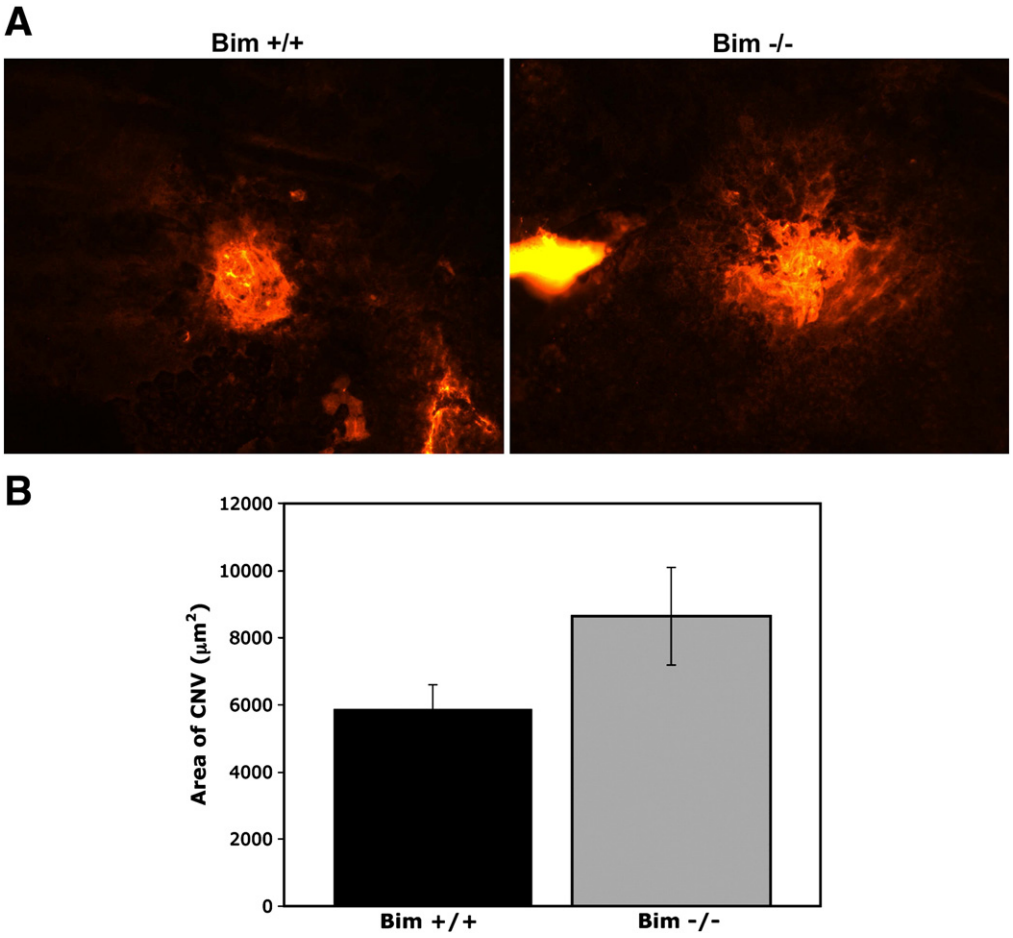


**Fig. 11.** Choroidal neovascularization occurs in the absence of bim. Choroidal neovascularization was induced in 6-week-old female bim+/+ and bim−/− mice by laser photocoagulation-induced rupture of Bruch's membrane. After 14 days, the eyes were removed and fixed in 4% paraformaldehyde. The eyes were sectioned at the equator, and the anterior half, the vitreous, and the retina removed. The remaining eye tissue was stained with anti-ICAM-2 to visualize the area of neovascularization (Panel A). Panel B is the quantitative assessment of the area of neovascularization ($P=0.1$). Please note choroidal neovascularization occurs in the presence or absence of bim. These experiments were repeated with at least 10 mice of each genotype.

bim. Thus, our data is consistent with retinal neovascularization and CNV being regulated in a different manner. Whether these differences in neovascularization are due to choroidal EC fenestration, hypoxia, or stage of development require further delineation. Alternatively, different bcl-2 family member death effectors may modulate choroidal versus retinal neovascularization. Thus, gaining a better understanding of the role bim plays in modulating ocular vascular homeostasis will give us new points of intervention.

## Acknowledgments

This work was supported in part by the grants University of Wisconsin Department of Pediatrics Research and Development Fund (CMS). CMS was funded, in part, by DK067120 from the National Institutes of Health. The authors wish to thank Dr. Nader Sheibani for critical reading of this manuscript, Robert Gordon for his assistance with the graphics, Terri DiMaio for technical assistance and Elizabeth Scheef for quantitative analysis of the data.

## References

Abutin, R.M., Chen, J., Lung, T.K., Lloyd, J.A., Sawyer, S.T., Harada, H., 2009. Erythropoietin-induced phosphorylation/degradation of BIM contributes to survival of erythroid cells. Exp. Hematol. 37, 151–158.

Bouillet, P., Metcalf, D., Huang, D.C., Tarlinton, D.M., Kay, T.W., Kontgen, F., Adams, J.M., Strasser, A., 1999. Proapoptotic Bcl-2 relative Bim required for certain apoptotic responses, leukocyte homeostasis, and to preclude autoimmunity. Science 286, 1735–1738.

Bouillet, P., Cory, S., Zhang, L.C., Strasser, A., Adams, J.M., 2001. Degenerative disorders caused by Bcl-2 deficiency prevented by loss of its BH3-only antagonist Bim. Dev. Cell 1, 645–653.

Bouillet, P., Robati, M., Bath, M., Strasser, A., 2005. Polycystic kidney disease prevented by transgenic RNA interference. Cell Death Differ. 12, 831–833.

Campochiaro, P.A., 2000. Retinal and choroidal neovascularization. J. Cell. Physiol. 184, 301–310.

Chen, J., Connor, K.M., Aderman, C.M., Smith, L.E., 2008. Erythropoietin deficiency decreases vascular stability in mice. J. Clin. Invest. 118, 526–533.

Chen, J., Connor, K.M., Aderman, C.M., Willett, K.L., Aspegren, O.P., Smith, L.E., 2009. Suppression of retinal neovascularization by erythropoietin siRNA in a mouse model of proliferative retinopathy. Invest. Ophthalmol. Vis. Sci. 50, 1329–1335.

Dias, S., Shmelkov, S.V., Lam, G., Rafii, S., 2002. VEGF165 promotes survival of leukemic cells by Hsp90-mediated induction of bcl-2 expression and apoptosis inhibition. Blood 99, 2532–2540.

Doonan, F., Donovan, M., Gomez-Vicente, V., Bouillet, P., Cotter, T.G., 2007. Bim expression indicates the pathway to retinal cell death in development and degeneration. J. Neurosci. 27, 10887–10894.

Dorrell, M.I., Aguilar, E., Friedlander, M., 2002. Retinal vascular development is mediated by endothelial filopodia, a preexisting astrocytic template and specific R–cadherin adhesion. Invest Ophthalmol. Vis. Sci. 43, 3500–3510.

Folkman, J., 2003. Angiogenesis and apoptosis. Semin. Cancer Biol. 13, 159–167.

Fruttiger, M., 2002. Development of the mouse retinal vasculature:angiogenesis versus vasculogenesis. Invest Ophthalmol. Vis. Sci. 43, 522–527.

Fruttiger, M., 2007. Development of the retinal vasculature. Angiogenesis 10, 77–88.

Giancotti, F.G., Ruoslahti, E., 1999. Integrin signaling. Science 285, 1028–1032.

Grutzmacher, C., Park, S., Elmergreen, T.L., Tang, Y., Scheef, E.A., Sheibani, N., Sorenson, C.M., 2010. Opposing effects of Bim and Bcl-2 on lung endothelial cell migration. Am. J. Physiol. Lung Cell. Mol. Physiol. 299, L607–20.

Huang, Q., Wang, S., Sorenson, C.M., Sheibani, N., 2008. PEDF-deficient mice exhibit an enhanced rate of retinal vascular expansion and are more sensitive to hyperoxia-mediated vessel obliteration. Exp. Eye Res. 87, 226–241.

Iervolino, A., Trisciuoglio, D., Ribatti, D., Candiloro, A., Biroccio, A., Zupi, G., del Bufalo, D., 2002. Bcl-2 overexpression in human melanoma cells increases angiogenesis through VEGF mRNA stabilization and HIF-1-mediated transcriptional activity. FASEB J. 10, 1453–1455.

Ito, M., Yoshioka, M., 1999. Regression of the hyaloid vessels and papillary membrane of the mouse. Anat Embryol. 200, 403–411.

Jimenez, B., Volpert, O.V., Crawford, S.E., Febbraio, M., Silverstein, R.L., Bouck, N., 2000. Signals leading to apoptosis-dependent inhibition of neovascularization by thrombospondin-1. Nat. Med. 6, 41–48.

Karsan, A., Yee, E., Poirier, G.G., Zhou, P., Craig, R.W., Harlan, J.M., 1997. Fibroblast groth factor-2 inhibits endothelial cell apoptosis by Bcl-2-dependent and independent mechanisms. Am. J. Pathol. 151, 1775–1784.

Kim, S., Bell, K., Mousa, S.A., Varner, J.A., 2000. Regulation of angiogenesis in vivo by ligation of integrin alpha5beta1 with the central cell-binding domain of fibronectin. Am. J. Pathol. 156, 1345–1362.

Kondo, S., Tang, Y., Scheef, E.A., Sheibani, N., Sorenson, C.M., 2008. Attenuation of retinal endothelial cell migration and capillary morphogenesis in the absence of Bcl-2. Am. J. Physiol. Cell Physiol. 294, C1521–30.

Linseman, D.A., Phelps, R.A., Bouchard, R.J., Le, S.S., Laessig, T.A., McClure, M.L., Heidenreich, K.A., 2002. Insulin-like growth factor-I blocks Bcl-2 interacting mediator of cell death (Bim) induction and intrinsic death signaling in cerebellar granule neurons. J. Neurosci. 22, 9287–9297.

Lofqvist, C., Andersson, E., Sigurdsson, J., Engstrom, E., Hard, A.L., Niklasson, A., Smith, L.E., Hellstrom, A., 2006. Longitudinal postnatal weight and insulin-like growth factor I measurements in the prediction of retinopathy of prematurity. Arch. Ophthalmol. 124, 1711–1718.

Lofqvist, C., Willett, K.L., Aspegren, O., Smith, A.C., Aderman, C.M., Connor, K.M., Chen, J., Hellstrom, A., Smith, L.E., 2009. Quantification and localization of the IGF/insulin system expression in retinal blood vessels and neurons during oxygen-induced retinopathy in mice. Invest. Ophthalmol. Vis. Sci. 50, 1831–1837.

Pierce, E.A., Foley, E.D., Smith, L.E., 1996. Regulation of vascular endothelial growth factor by oxygen in a model of retinopathy of prematurity. Arch. Ophthalmol. 114, 1219–1228.

Pollman, M.J., Naumovski, L., Gibbons, G.H., 1999. Endothelial cell apoptosis in capillary network remodeling. J. Cell. Physiol. 178, 359–370.

Reed, J.C., Zha, H., Aime-Sempe, C., Takayama, S., Wang, H.G., 1996. Structure function analysis of bcl-2 family proteins. Mechanisms of lymphocyte activation and immune regulation VI, pp. 99–112.

Sheibani, N., Scheef, E.A., DiMaio, T.A., Wang, Y., Kondo, S., Sorenson, C.M., 2007. Bcl-2 expression modulates cell adhesion and migration promoting branching of ureteric bud cells. J. Cell. Physiol. 210, 616–625.

Smith, L.E., Wesolowski, E., McLellan, A., Kostyk, S.K., D'Amato, R., Sullivan, R., D'Amore, P.A., 1994. Oxygen-induced retinopathy in the mouse. Invest. Ophthalmol. Vis. Sci. 35, 101–111.

Sorenson, C.M., 2004. Bcl-2 family members and disease. Biochim. Biophys. Acta 1644, 169–177.

Sorenson, C.M., Sheibani, N., 2002. Sustained activation of MAPK/ERK's signaling pathway in cystic kidneys from Bcl-2−/− mice. Am. J. Physiol. 283, F1085–F1090.

Stone, J., Itin, A., Alon, T., Pe'er, J., Gnessin, H., Chan-Ling, T., Keshet, E., 1995. Development of retinal vasculature is mediated by hypoxia-induced vascular endothelial growth factor (VEGF) expression by neuroglia. J. Neurosci. 15, 4738–4747.

Stone, J., Chan-Ling, T., Pe'er, J., Itin, A., Gnessin, H., Keshet, E., 1996. Roles of vascular endothelial growth factor and astrocyte degeneration in the genesis of retinopathy of prematurity. Invest. Ophthalmol. Vis. Sci. 37, 290–299.

Strasser, A., O'Connor, L., Dixit, V.M., 2000. Apoptosis signaling. Annu. Rev. Biochem. 69, 217–245.

Vaux, D.L., Cory, S., Adams, J.M., 1988. Bcl-2 gene promotes haemopoietic cell survival and cooperates with c-myc to immortalize pre-B cells. Nature 335, 440–442.

Walsh, K., Smith, R.C., Kim, H.S., 2000. Vascular cell apoptosis in remodeling, restenosis, and plaque rupture. Circ. Res. 87, 184–188.

Wang, S., Wu, Z., Sorenson, C.M., Lawler, J., Sheibani, N., 2003. Thrombospondin-1-deficient mice exhibit increased vascular density during retinal vascular development and are less sensitive to hyperoxia-mediated vessel obliteration. Dev. Dyn. 228, 630–642.

Wang, S., Sorenson, C.M., Sheibani, N., 2005. Attenuation of retinal vascular development and neovascularization during oxygen-induced ischemic retinopathy in Bcl-2−/− mice. Dev. Biol. 279, 205–219.

Ziehr, J., Sheibani, N., Sorenson, C.M., 2004. Alterations in cell adhesive and migratory properties of proximal tubule and collecting duct cells from bcl-2−/− mice. Am. J. Physiol. 287, F1154–F1163.